Structural transformation and vibrational properties of BaC₂ at high pressure

I. Efthimiopoulos,[1] K. Kunc,[1,*] G. V. Vazhenin,[1,2,†] E. Stavrou,[1] K. Syassen,[1,‡] M. Hanfland,[3] St. Liebig,[4] and U. Ruschewitz[4]

[1]*Max-Planck-Institut für Festkörperforschung, Heisenbergstraße 1, D-70569 Stuttgart, Germany*
[2]*Institut für Anorganische Chemie, Universität Stuttgart, Pfaffenwaldring 55, D-70569 Stuttgart, Germany*
[3]*European Synchrotron Radiation Facility, F-38043 Grenoble, France*
[4]*Department für Chemie, Universität zu Köln, Greinstraße 6, D-50939 Köln, Germany*
(Received 24 October 2011; published 9 February 2012)

We show that the ambient-pressure tetragonal phase of BaC₂ (CaC₂-type, space group $I4/mmm$), with sixfold coordination of Ba atoms and C₂ dumbbells, transforms reversibly to a new structure type at 4 GPa; it is an eight-coordinated rhombohedral modification (space group $R\bar{3}m$), which can be viewed as a distorted variant of the CsCl-type structure. X-ray diffraction experiments further reveal an irreversible amorphization of BaC₂ above 30 GPa. The possibility of a pressure-induced polymerization of isolated C₂ dumbbells into a network is considered. We also study lattice dynamics of both crystalline phases by Raman measurements, and compare the experimental observations on structures, phonons, and the first phase transition with the results of *ab initio* calculations. The latter also supply additional data on atomic positions, interatomic distances, and the volume-dependent equation of state (total energy and pressure).

I. INTRODUCTION

While elemental carbon exists in the form of network structures such as graphite or diamond, its neighbors in the periodic table, oxygen and nitrogen, form gases of diatomic molecules at ambient conditions, with oligomerization (oxygen[1]) and polymerization (nitrogen[2]) observed only at high pressure. A similar tendency toward formation of oligomeric and polymeric networks is quite strong in metal carbides compared to related oxides and nitrides as well. While isolated oxide O^{2-} and nitride N^{3-} ionic species are more common structural motifs compared to oligomeric peroxide (O_2^{2-}), superoxide (O_2^-), azide (N_3^-), and pernitride (N_2^{2-}) groups, structural chemistry of carbides, especially those with electropositive metals, tend to feature oligomeric or polymeric carbon networks. In a simple ionic picture, this can be related to the electrostatic instability of the carbide anion C^{4-} in addition to the stability of carbon-carbon bonds in comparison to those for nitrogen and oxygen.

The most common dimeric anion with carbon atoms is C_2^{2-} with a triple bond between the two carbon atoms. Compounds containing the dicarbide anion can be viewed as salts of acetylene C₂H₂ (ethyne) and hence are also referred to as acetylides or ethynides. Since C_2^{2-} possesses a closed-shell electronic configuration and is isoelectronic to the N₂ molecule, most ionic acetylides are semiconductors or insulators. Deviations from this electron count in dicarbides are quite of interest as well since these can result in noteworthy physical properties such as superconductivity in YC₂,[3] mixed-valence behavior in YbC₂ at ambient conditions,[4] and possibly a change in the Eu valence state in EuC₂ under pressure.[5]

Even though the main structural aspects of metal acetylides have been long established, crystal structures of a number of alkali and alkaline-earth metal acetylides have been investigated in more detail recently.[6] Structural transformations in acetylides such as CaC₂ and BaC₂ have been studied as a function of temperature.[7,8] The orientation of the dicarbide dumbbell within the solid was emphasized as the main structure-determining factor.

It is of considerable interest to study the effect of pressure on the crystal structures of acetylides as well. First, pressure-induced reorientation of the dicarbide dumbbells similar to those in temperature-induced phase transitions are possible as has already been shown for LaC₂ in its CaC₂-type to ThC₂-type phase change.[9,10] To our knowledge, only one other pressure-induced structural transformation has been identified for dicarbides, namely, the CaC₂ type to hexagonal transition of UC₂.[11] Further, the possibility of NaCl-like-to-CsCl-like pressure-induced phase transition, involving a major change in coordination, has been demonstrated recently for related barium peroxide BaO₂.[12] Finally, the latter study also suggested a possibility of polymerization of the peroxide O_2^{2-} groups at much higher pressures. While still hypothetical for oxides, this possibility is more realistic for carbides due to the above-mentioned stability of oligomeric and polymeric carbon networks. Such polymerization might thus be a link between the acetylides and other carbides, for example, graphite-related superconductors such as YC₆ and CaC₆.[13]

This paper reports a high-pressure study of barium dicarbide. At ambient conditions, the compound crystallizes in a rocksalt-related tetragonal phase (cf. Fig. 1). Pressure-induced structural phase transitions are detected and characterized by synchrotron x-ray diffraction and Raman spectroscopy (Sec. II). The two main findings are the reversible transition to a phase of CsCl-related coordination, followed by a nonreversible transition to a disordered phase at higher pressure.

A few theoretical works exist on BaC₂[14–17]; all are based on the density functional theory. Reference 14 focuses on electronic properties of the bonds and their topology [electron localization function (ELF)]. It also deals with vibrational frequencies, dipole moments, and bond lengths. In Ref. 15, different chain and sheet structures of several cyanides and dicarbides are considered at zero pressure. Reference 16 deals with electronic properties (band structure, density of states, electronic charge distribution) at zero pressure of two isomers of BaC₂: the tetragonal ($I4/mmm$) and monoclinic one
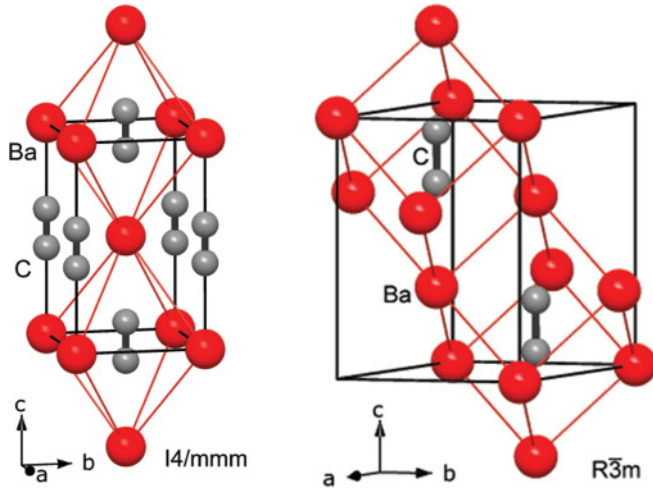
FIG. 1. (Color online) Left: Crystal structure of the ambient-pressure tetragonal phase (space group $I4/mmm$, $Z = 2$) of BaC_2. The large (red) and small (gray) spheres correspond to Ba and C atoms, respectively. In this structure, the Ba atoms form an octahedral environment around the C_2 dumbbells. Right: Crystal structure of the high-pressure rhombohedral phase (space group $R\bar{3}m$, $Z = 3$) of BaC_2. In this structure, the Ba atoms form a distorted cube around the C_2 dumbbells.

($C2/c$). Finally, Ref. [17] considers pressure-induced carbon network formation for selected alkaline-earth dicarbides. We present results of calculations for BaC_2 under pressure (Sec. III) that relate directly to our experimental findings about phase stability and vibrational properties.

II. EXPERIMENTAL INVESTIGATIONS

A. Methods

A polycrystalline powder of BaC_2 was prepared according to the previously reported procedure.[8] The sample was handled under argon atmosphere in order to avoid reactions with moisture, oxygen, or carbon dioxide from the air. An x-ray diffraction (XRD) pattern measured at ambient pressure on BaC_2 sealed in a glass capillary (STOE STADI-P diffractometer with Mo-Kα radiation) was indexed with a tetragonal body-centered unit cell based on the positions of 20 diffraction maxima, yielding

$$a = 4.399(1) \text{ Å}, \ c = 7.120(3) \text{ Å}, \ V_{cell} = 137.8(1) \text{ Å}^3.$$

These unit-cell parameters agree with previous results reported for BaC_2.[8]

In situ high-pressure diffraction experiments were conducted at room temperature with a gasketed diamond anvil cell (DAC). Pressures were measured by the well-established ruby luminescence method.[18] Silicon oil was employed as a pressure-transmitting medium. Diffraction data were collected at the ID09A beamline of the European Synchrotron Radiation Facility, Grenoble, using a MAR555 flat panel detector. The monochromatic x-ray beam (wavelength $\lambda = 0.4146$ Å) was collimated to a nominal diameter of 30 μm. In order to improve powder averaging, the DAC was rocked by $\pm 3°$. The scanned two-dimensional diffraction patterns were corrected for tilt and scanner distortions and converted to intensity- *vs* $- 2\theta$

data using the FIT2D software.[19] Rietveld refinements of the crystal structures were performed using the GSAS program.[20]

In situ Raman spectra were recorded at room temperature (RT) with a microscope laser Raman system (Jobin-Yvon, LabRam) operating with excitation lines $\lambda = 632.82$ and 532 nm at 1 mW. Pressure was controlled by the ruby luminescence method as well. No pressure-transmitting medium was employed in order to avoid possible interference from its luminescence and reactions at the sample surface.

B. Structural properties under pressure

At ambient conditions, BaC_2 crystallizes in the tetragonal CaC_2-type structure.[21] (space group $I4/mmm$, $Z = 2$, Fig. 1, left). The structure is typically viewed as a tetragonally distorted NaCl-type arrangement, with Ba atoms on the Na site. The C_2 dumbbells occupy the Cl site, all parallel to each other and to the c axis of the tetragonal structure, thus resulting in an elongated coordination octahedron.

Typical XRD patterns at various pressures are shown in Fig. 2. The onset of the phase transition is seen at the pattern
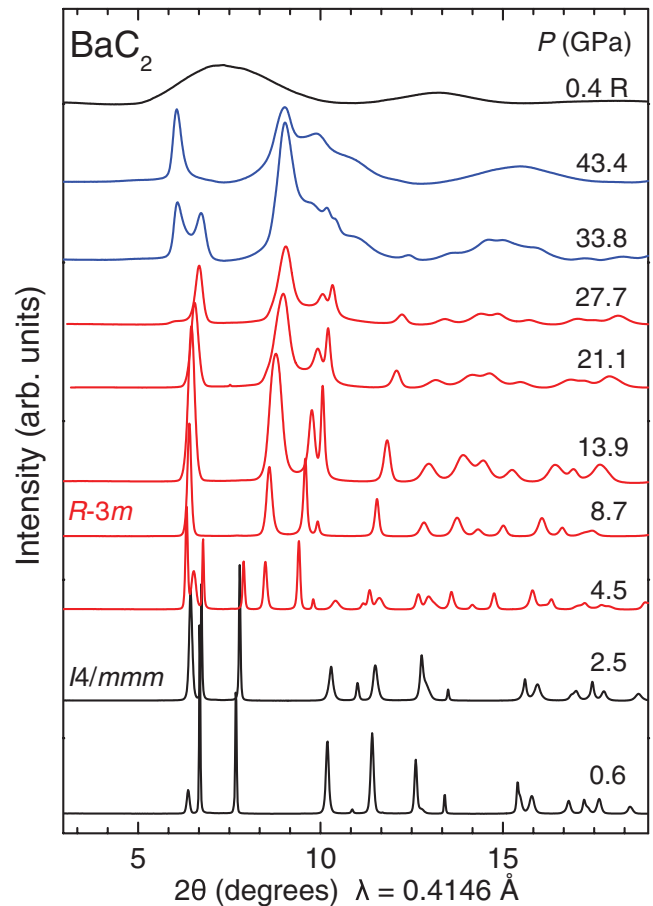
FIG. 2. (Color online) X-ray diffraction patterns of BaC_2 at selected pressures ($\lambda = 0.4146$ Å, $T = 300$ K). The diagram at 4.5 GPa corresponds to a phase mixture of the ambient-pressure tetragonal ($I4/mmm$) and the high-pressure rhombohedral ($R\bar{3}m$) phases. At about 30 GPa, the rhombohedral phase is followed by a sluggish transformation to a second high-pressure phase, the structure of which is not identified. Upon pressure release, the sample turns amorphous.
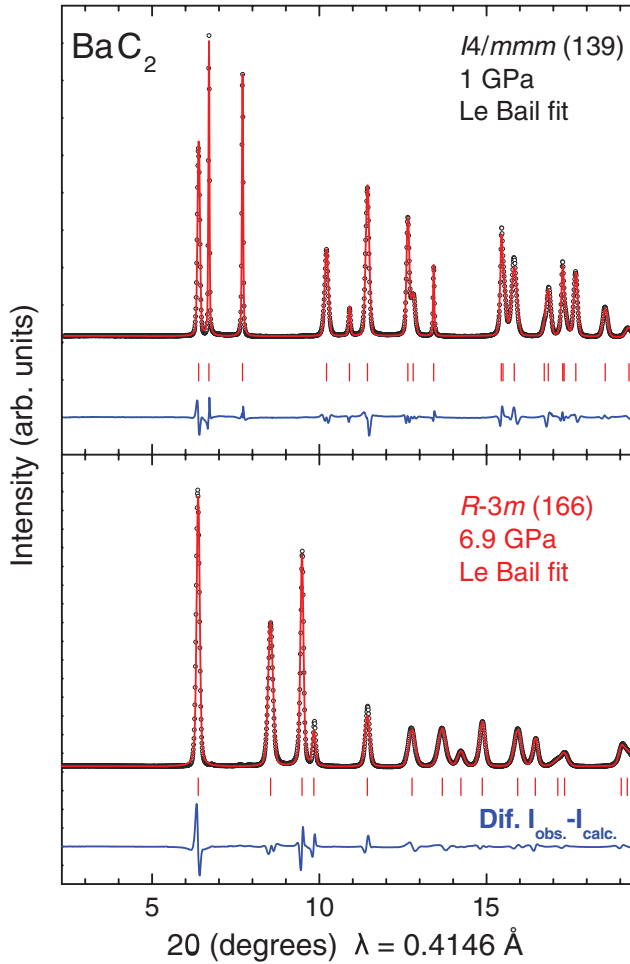
FIG. 3. (Color online) XRD patterns of BaC_2 at 1 GPa (top, $I4/mmm$) and at 6.9 GPa (bottom, $R\bar{3}m$). Symbols correspond to the measured profile, the red solid lines drawn through data represent the results of Le Bail refinements. The difference curves (blue lines) are shown also. Vertical ticks mark positions of Bragg peaks.

TABLE I. Refined crystallographic data at two different pressures for the ambient-pressure tetragonal and the high-pressure rhombohedral modifications of BaC_2 (hexagonal setting). The site notation follows Wyckoff residuals R as defined in GSAS (Ref. [20]). The values of z are not refined, but are taken from our calculations at the quoted volumes. See text for the lattice parameters of our sample at zero pressure.

	Tetragonal	Rhombohedral
Space group	$I4/mmm$ (139)	$R\bar{3}m$ (166)
Pressure (GPa)	1.0	6.9
a (Å)	4.3643	5.0166
c (Å)	7.0966	7.2524
V_{cell} (Å^3)	135.17	158.07
Z	2	3
R_p, wR_p	0.030, 0.049	0.062, 0.085
Ba site	$2a$ (0,0,0)	$3a$ (0,0,0)
C site	$4e$ (0,0,z)	$6c$ (0,0,z)
	$z = 0.4123$	$z = 0.4133$

Representative fits of the experimentally observed diffraction patterns based on the ambient-pressure and high-pressure BaC_2 structures are shown in Fig. 3. The corresponding structural details are summarized in Table I. Full structural refinement was not possible due to stress-induced preferred orientation effects and strongly anisotropic peak broadening.

The pressure dependence of the lattice parameters and volume per formula unit of BaC_2 in the ambient- and high-pressure phases are shown in Fig. 4. Reliable fits could be obtained for the data collected up to 14 GPa. Diffraction diagrams taken at higher pressure are significantly broadened. Presumably, this effect is caused by nonhydrostaticity of the pressure medium.

Throughout this paper, PV data (experimental and calculated) are fitted by the Holzapfel AP1 empirical equation of state (EOS) expression[25]

$$P(x) = 3\,B_0\,\frac{1-x}{x^5}\,\exp[\eta\,(1-x)],$$
$$x = \left(\frac{V}{V_0}\right)^{1/3}, \quad \eta = \frac{3}{2}(B_0' - 3). \quad (1)$$

By taking the PV data for the tetragonal $I4/mmm$ phase up to 4 GPa, we obtain

$$V_0 = 68.9(1)\ \text{Å}^3, \quad B_0 = 49(2)\ \text{GPa}$$

for $B_0' = 4$ fixed. The PV data for the $R\bar{3}m$ phase, also approximated by the AP1 form, give

$$V_t = 53.8(2)\ \text{Å}^3, \quad B_t = 85(5)\ \text{GPa}$$

at the reference pressure $P_t = 4.5$ GPa ($B_t' = 4$ fixed). The first-order transformation to the high-pressure rhombohedral phase is accompanied by a relative volume decrease of $\Delta V/V = -15\%$.

Further pressure increase results in another structural phase transformation to an as yet unidentified high-pressure polymorph of BaC_2 (BaC_2-HP2), with the transformation being complete only at the highest pressure applied (43.4 GPa). Upon pressure decrease, BaC_2-HP2 does not transform back to rhombohedral BaC_2-HP1 or the tetragonal ambient-pressure

collected at 4.5 GPa, with the high-pressure modification present as a single phase from 6.9 to 27 GPa. The set of new diffraction peaks could be indexed with a rhombohedral unit cell (space group $R\bar{3}m$, $Z = 3$, hexagonal setting). The proposed structural model for this phase, denoted BaC_2-HP1, is shown in Fig. 1 (right). This crystal structure can be viewed as a CsCl-type arrangement, in which, in analogy to the ambient-pressure phase, Ba atoms occupy the alkali metal sites and C_2 dumbbells the halogen atom sites. Again, all dumbbells lie parallel to each other and to the unique c axis (hexagonal setting) of the rhombohedral structure. The resulting coordination of the dumbbells is eightfold.

Formally, the structure of BaC_2-HP1 represents a new structural type. However, it is closely related to, for example, the rhombohedral sodium azide NaN_3 (Ref. [22]) and $CaCN_2$ (Ref. [23]) where the linear triatomic azide or carbodiimide groups are the equivalent of the diatomic dicarbide dumbbells in rhombohedral BaC_2. Further, the structure has been a candidate in a recent simulated annealing study of the enthalpy landscape of CaC_2 where it is predicted to become stable at a pressure of 30 GPa.[24]

FIG. 4. (Color online) Lattice parameters and volume per formula unit for the low- and high-pressure phases of BaC_2. Solid lines represent guides to the eye. The dashed lines mark the onset of the structural transition.

phase. Instead, an apparent amorphization takes place with no clear diffraction peaks present any more below 3 GPa.

A possible mechanism for the HP1 to HP2 transformation of BaC_2 might include polymerization of the dicarbide dumbbells into a network. This hypothesis is consistent with the observed pressure for this transformation, corresponding to the upper limit for the existence of multiple bonding between carbon atoms.[26] Such polymerization would explain the irreversibility of this phase transformation. Incidentally, the arrangement of carbon atoms in BaC_2-HP1 corresponds to a distorted cubic diamond lattice when nearest-neighbor contacts between the dumbbells are considered. However, the inter-dumbbell distance is so large that the relation to diamond is geometrical only.

As for the HP2 phase, we can not be sure that it is a single phase. The possibility of a phase separation is not ruled out because at, say, 45 GPa the sum of the atomic volumes of one atom in Ba metal [~ 22 Å^3 (Ref. 27)] and two carbons in diamond (estimated as $\sim 2 \times 5.2$ Å^3 from its compressibility) is much smaller than the extrapolated volume of BaC_2-HP1 (~ 39.6 Å^3). In this context, we also note that the diffraction diagram taken after release of pressure at 0.4 GPa shows two broad features at d values of about $d = 3.16(4)$ and $d = 1.82(5)$ (ratio square root of 3). These features are, however, not easily reconciled with the lattice parameter $a = 5.02$ Å of elemental bcc barium at ambient pressure.

C. Raman scattering under pressure

Raman spectra of BaC_2 are shown in Fig. 5(a), the frequencies of Raman features are plotted in Fig. 5(b) as a

function of pressure, and quantitative information on the effect of pressure on Raman mode frequencies of BaC_2 is collected in Table II.

For the ambient-pressure tetragonal phase ($I4/mmm$), two first-order Raman modes are expected, having E_g and A_{1g} symmetry, analogous, e.g., to those in tetragonal BaO_2.[28,29] The low-frequency E_g mode is twofold degenerate and corresponds to the librational motion of the C_2 units. The high-frequency A_{1g} mode is a stretching motion of the C_2 group. These two modes are observed in the zero-pressure Raman spectra at 193 and 1833 cm^{-1}, respectively. The A_{1g} mode dominates the spectrum, and the E_g mode is much weaker [cf. Fig. 5(a)].

Upon pressure increase, a clear change of the Raman spectra is observed at about 4 GPa and it is attributed to the tetragonal-to-rhombohedral structural transition, in accordance with the results of the XRD study. For the rhombohedral $R\bar{3}m$ phase, two Raman modes are expected as well (see theoretical results below): a low-frequency mode of E_g symmetry and a higher-lying A_{1g} mode. Like in tetragonal BaC_2, the A_{1g} mode corresponds to the C–C stretching motion. It appears at frequencies lower than that of the respective A_{1g} mode of the tetragonal phase and exhibits a similar shift with pressure [see Figs. 5(a) and 5(b)]. The E_g mode corresponds to C_2 librations, similar to the E_g mode in the tetragonal phase.

With further increasing pressure, the E_g mode of phase II broadens significantly, and above 12 GPa one can not assign any more a well-defined frequency value. At a pressure of about 30 GPa, the sharp Raman signature of the C–C stretch mode is lost. This indicates a pressure-driven disruption
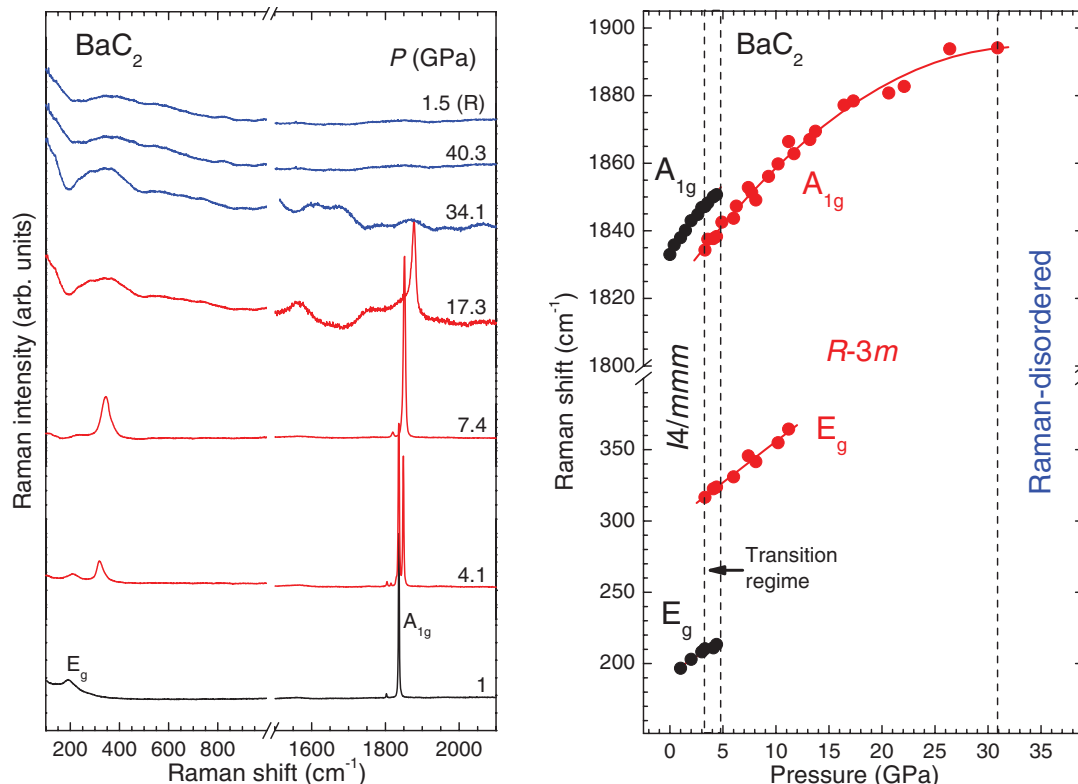
FIG. 5. (Color online) Left: Raman spectra of BaC_2 at various pressures. The laser excitation wavelength is $\lambda = 633$ nm. The spectra correspond to the tetragonal $I4/mmm$ phase (1 GPa), a mixed-phase point (4.1 GPa), the rhombohedral $R\bar{3}m$ phase (7.4 GPa, 17.3 GPa), and disordered phases. Right: Frequencies of the observed Raman modes of BaC_2 as a function of pressure. Lines represent linear or quadratic relations fitted to the data. The vertical dashed lines mark the onset (and width) of the structural phase transitions as seen in the Raman scattering experiments.

of the C–C dumbbell unit. Above this point (spectrum at 34.1 GPa), the Raman spectrum consists of several broad bands. Assignment to possible fragmented carbon units would be speculative at this point. At about 40 GPa, the Raman spectrum becomes rather featureless. This remains unchanged when releasing pressure to almost zero (spectrum at 1.5 GPa). So, Raman spectroscopy indicates a pressure-induced disorder, which is irreversible. The disorder evidenced by the Raman response at around 40 GPa may be of local

TABLE II. Assignment (Refs. 28,29) frequencies, pressure coefficients, and mode Grüneisen parameters γ of the Raman modes of BaC_2. The mode frequencies and their slopes refer to reference pressures of 0 and 3.3 GPa for the $I4/mmm$ and the $R\bar{3}m$ phases. The linear pressure coefficients $\partial\omega/\partial P$ were obtained by linear and quadratic fits to the measured data. The values of the mode Grüneisen parameters γ are obtained using $\gamma = (B/\omega)(\partial\omega/\partial P)$, where $B = 49$ GPa for the $I4/mmm$ phase and $B = 80$ GPa for the high-pressure $R\bar{3}m$ phase at 3.3 GPa.

Phase	Mode	ω_r (cm^{-1})	$\partial\omega/\partial P$ (cm^{-1}/GPa)	γ
$I4/mmm$	E_g	193	4.7	1.2
$P_r = 0$ GPa	A_{1g}	1833	5.4	0.14
$R\bar{3}m$	E_g	317	5.8	1.5
$P_r = 3.3$ GPa	A_{1g}	1834	4.4	0.19

nature. That is, it is considered to not be in disagreement with the persistence of long-range order as is indicated by the relatively sharp low-angle diffraction peak seen near 40 GPa.

III. COMPUTATIONAL RESULTS

A. Computational details

The numerical work presented here proceeds along the same lines as, e.g., in Ref. 12. We employ density functional theory (DFT) in the generalized gradient approximation (GGA),[30] a plane-wave basis, and PAW potentials (projector augmented waves)[31,32] using the VASP codes.[33,34] The $5s^2$, $5p^6$, and $6s^2$ states of barium are treated as valence states (i.e., 10 electrons are dealt with explicitly, corresponding to the PAW potential labeled as Ba_sv), and for carbon the potential denoted as C_h ($h = $ "hard") in the database[32,34] is chosen. A plane-wave cutoff $E_{pw} = 875$ eV is used and the k-point sampling of the reciprocal space is performed on $6 \times 6 \times 6$ meshes of the Monkhorst-Pack type[35] (129 and 28 irreducible k points in, respectively, tetragonal and rhombohedral phases). Insulating behavior was assumed and confirmed by inspection of the electronic band structures for both phases throughout the studied pressure range. The calculations on both structures are carried out based on the periodicity defined by the respective primitive unit cells containing one formula unit BaC_2 each. For each volume, the ratios of the unit-cell

parameters and the free internal atomic parameter of carbon are optimized with respect to the total energy. Pressure P is evaluated directly from the DFT with the aid of stress theorem.[36]

B. Crystal structures of BaC_2 and their transformations

The computed $E(V)$ and $P(V)$ equations of state are shown in Fig. 6. These data are then converted into model EOS parameters reported in Table III. Both the calculated $E(V)$ and
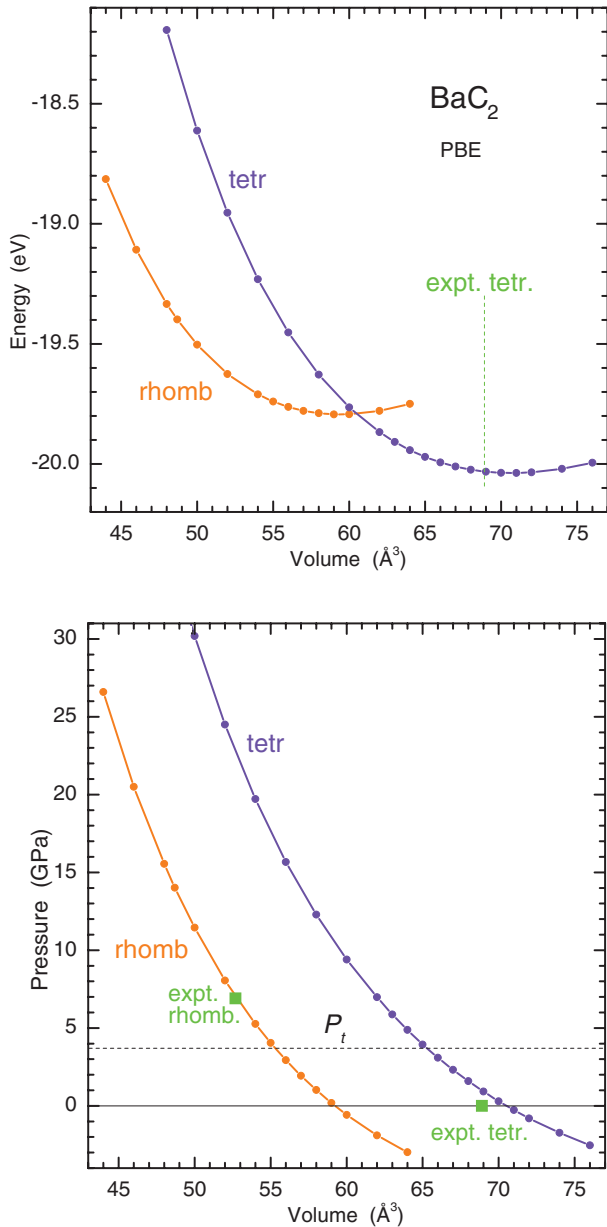
FIG. 6. (Color online) Calculated $E(V)$ and $P(V)$ equations of state for the tetragonal ($I4/mmm$) and rhombohedral ($R\bar{3}m$) phases of BaC_2 (small dots). Both volume and energy refer to one formula unit of BaC_2. The solid lines represent the fits of the EOS expression (1) and its integrated analytical form. Experimental data for the respective phases at zero pressure and 6.8 GPa (cf. Table I) are indicated by square symbols. The horizontal dotted line labeled P_t marks the calculated phase transition pressure.

TABLE III. The theoretical equation-of-state parameters of BaC_2 in both structures. The least-squares fits to the calculated data by the Holzapfel AP1 empirical EOS Eq. (1) and its integrated analytical form are based on 17 volumes in the interval 52.0 to 74.0 Å³/BaC_2 in the tetragonal structure, and on 13 volumes in the interval 44.0 to 62.0 Å³/BaC_2 in the rhombohedral phase. The uncertainties quoted correspond to 90% confidence limits. All volumes V_0 refer to the *primitive* unit cells hosting one formula unit of BaC_2 each.

Phase	Data	V_0 (Å³)	B_0 (GPa)	B_0'
Tetragonal	$E(V)$	70.705(9)	39.78(11)	4.64(2)
	$P(V)$	70.516(20)	40.21(2)	4.63(3)
Rhombohedral	$E(V)$	59.401(28)	45.66(49)	4.53(7)
	$P(V)$	59.234(12)	46.22(17)	4.51(2)

$P(V)$ data were used and the EOS parameters (equilibrium volume V_0, bulk modulus B_0, and pressure derivative B_0') quoted in Table III refer to the AP1 expression (1) or its integrated form, which in this particular case offers the best fits and/or the best consistency for the theoretical $E(V)$ and $P(V)$ data. The two $E(V)$ equations of state intersect each other, and the calculation of enthalpies situates the first-order tetragonal → rhombohedral transition at pressure $P_t = 3.7$ GPa; the volumes per formula unit at the transition are 65.280 Å³ for tetragonal and 55.314 Å³, so the volume contraction is -15.3%. The rhombohedral structure is the stable modification above 3.7 GPa, in a very good agreement with both XRD and Raman results.

The computed crystallographic data and their variation with volume are shown in Fig. 7: the lattice parameters, their ratios, the C–C distance within the dumbbell, and the two shortest Ba–C distances. In general, the calculated results are in reasonable agreement with the available experimental data. Concerning bond distances, the theoretical results supply information that is missing from the experimental structure characterization. The C–C distance is related to the only free internal parameter for the carbon atoms in the tetragonal and rhombohedral structures. Figure 7(d) illustrates that the shortest Ba–C distances increase at the phase transition, as is typical of a pressure-driven NaCl-type to CsCl-type phase transition.

C. Test for monoclinic distortion

Because of peak broadening, our diffraction data taken above 14 GPa can not fully rule out a small monoclinic distortion of the rhombohedral high-pressure phase. Hence, we attempted to optimize the crystal structure of BaC_2 in an (assumed) monoclinic structure (space group $C2/m$, No. 12), viz., at formula volumes of $V = 46.0, 48.7, 50.0,$ and 54.0 Å³/BaC_2. Rather than dealing with the conventional unit cell (Pearson symbol $mC6$, a,b,c,β,u,w) we worked on a primitive translational unit with volume $0.5abc \sin \beta$ and one BaC_2 unit per cell. The k-point mesh $6 \times 6 \times 8$ leading to 84 k points was employed here.

Displaying the resulting optimized monoclinic lattices graphically, it becomes straightforward to recognize the
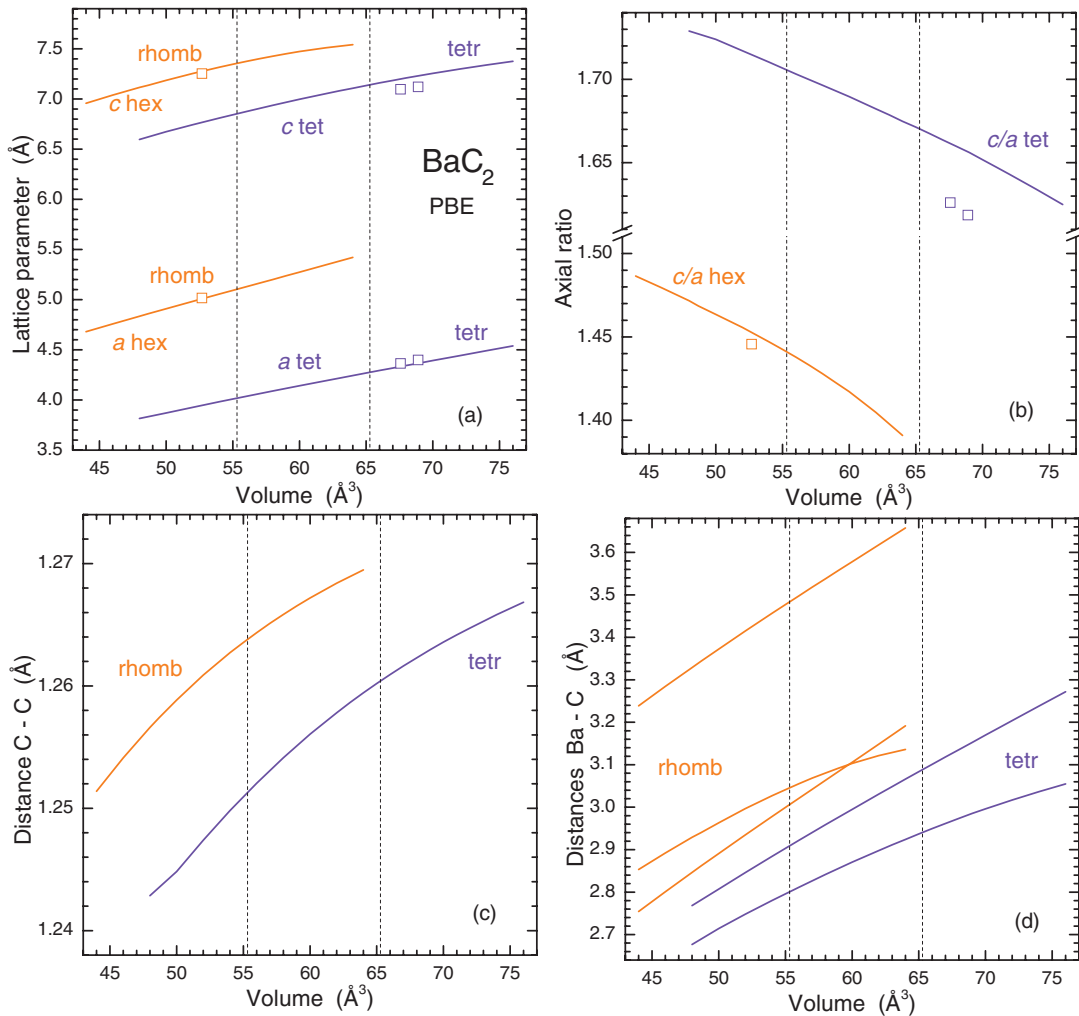
FIG. 7. (Color online) The theoretically optimized structural parameters of the tetragonal ($I4/mmm$) and rhombohedral ($R\bar{3}m$) phases of BaC$_2$ as functions of volume per formula unit (solid lines): (a) lattice parameters, (b) axial ratios, (c) C–C distance, and (d) Ba–C distances. Vertical dashed lines mark the calculated volumes at the phase transition. Selected experimental data for lattice parameters and axial ratios are indicated by open squares.

rhombohedral structure in which the basic rhombohedra are only *very slightly* deformed. For instance, at the volume $V = 50.0$ Å^3/BaC$_2$ the lattice translations $|\mathbf{a_i}|$ connecting the nearest Ba–Ba atoms were found to be 3.7110, 3.7105, and 3.7105 Å, which compares with $|\mathbf{a_i}| = 3.7110$ Å obtained in the rhombohedral structure at the same volume. Similarly, the "deformed rhombohedral angles" were calculated as 82.95°, 82.85°, and 82.85°, while they are 82.83° in the corresponding "perfect" rhombohedral structure. The C–C triple-bond length of 1.2587 Å found for the monoclinic phase is practically identical with 1.2589 Å obtained for the rhombohedral phase. A similar situation is found at other volumes ($V = 46$, 48.7, 54 Å^3): the spreads in Ba–Ba distances and Ba–Ba–Ba angles never exceeded 0.0009 Å and 0.12°. The energies calculated in both structures, at the four volumes, are found to differ by 0.2 to 0.7 meV/BaC$_2$ (the monoclinic being always higher in energy), which is probably smaller than the accuracy we can expect from this type of calculation. In other words, the energies of both structures are the same and the monoclinic high-pressure phase of BaC$_2$ is nothing but

at most an "infinitesimal" deformation of the rhombohedral structure.

D. Zone-center phonons in BaC$_2$

The structural transition visualized by the calculations above is reflected in the behavior of phonons. We calculated the frequencies of the Raman-active modes using the density-functional perturbation heory (DFPT),[37] as implemented in the VASP codes. Some of the results (particularly the behavior of the E_g mode in tetragonal structure) were checked by the calculations proceeding *via* forces directly (Hessian matrix). The relevant modes in both structures are either the C–C bond stretching (A_{1g}) or C–C-libration (E_g).

The frequencies evaluated for different *calculated* pressures are shown in Fig. 8 for the two structures, with related experimental results (measured frequencies versus *experimental* pressures) shown as an overlay. The calculations reproduce the C–C stretching frequencies, their pressure dependence, and the softening of the C–C stretching mode at the tetragonal-to-rhombohedral phase transition. The E_g mode frequency
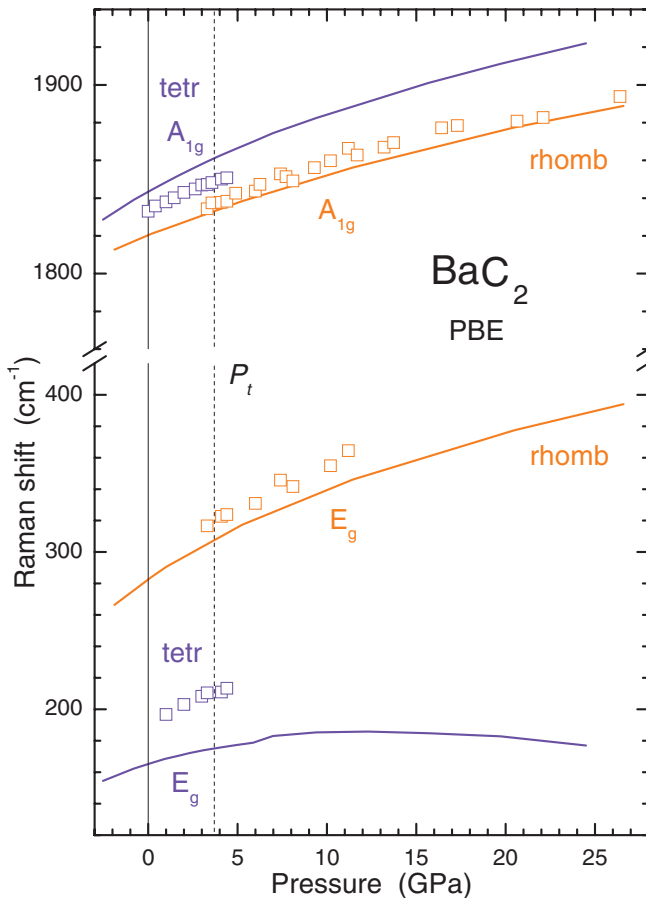
FIG. 8. (Color online) The theoretically calculated frequencies of the Raman-allowed mode of BaC_2 for the tetragonal and rhombohedral modifications as a function of calculated pressure (solid lines). The dashed vertical line marks the calculated phase transition pressure. Measured Raman mode frequencies versus experimental pressure are shown by open symbols.

of the rhombohedral phase is also well reproduced. The E_g mode frequency of the tetragonal phase comes out a bit too low when compared to the experiment. A possible explanation

could be an anharmonic upward shift, which is not included in the theoretical description. A similar effect with a low-lying E_g mode was noticed for both structures of BaO_2.[12]

IV. SUMMARY

Near 4 GPa, barium dicarbide BaC_2 undergoes a pressure-induced structural phase transformation, which may be viewed as an analog of the NaCl-to-CsCl–type transition. The local coordination number of the dumbbells built from the carbon atoms increases from six to eight. This structural behavior is similar to the previously studied barium peroxide BaO_2.[12] In the case of BaC_2, however, a different crystal structure is observed for the high-pressure phase. Actually, it corresponds to a new structure type.

Our *first-principles* calculations support the proposed structural model for the first high-pressure phase and the calculated results are essentially consistent with the observed parameters of the structural transformation. Different from BaO_2, BaC_2 is observed to undergo another phase change upon increasing pressure beyond 30 GPa, resulting in an as yet unidentified phase. Hypothetically, this irreversible phase change might involve polymerization of isolated dicarbide groups into extended networks or at least fragments. Loss of the Raman signal corresponding to the triple bond within the dicarbide unit in the course of this second transformation can be viewed as an additional argument in favor of the polymerization hypothesis. A more detailed characterization of the structural properties of BaC_2 at pressure above 30 GPa is left to future investigations involving *in situ* temperature treatment.

*Physique des Milieux Denses, IMPMC, CNRS-UMR7590 and Université Pierre et Marie Curie, Boîte courrier 115, 4 pl. Jussieu, F-75252 Paris-Cedex 05, France; karel.kunc@upmc.fr

†grigory.vazhenin@googlemail.com

‡k.syassen@fkf.mpg.de

[1] L. F. Lundegaard, G. Weck, M. I. McMahon, S. Desgreniers, and P. Loubeyre, Nature (London) **443**, 201 (2006).

[2] M. I. Eremets, A. G. Gavriliuk, I. A. Trojan, D. A. Dzivenko, and R. Boehler, Nat. Mater. **3**, 558 (2004).

[3] A. L. Giorgi, E. G. Szklarz, M. C. Krupka, T. C. Wallace, and N. Krikoria, J. Less-Common Met. **14**, 247 (1968).

[4] P. Link, P. Glatzel, K. Kvashnina, R. I. Smith, and U. Ruschewitz, Inorg. Chem. (Washington, DC, US) **50**, 5587 (2011).

[5] D. Wandner, P. Link, O. Heyer, J. Mydosh, M. A. Ahmida, M. M. Abd-Elmeguid, M. Speldrich, H. Lueken, and U. Ruschewitz, Inorg. Chem. (Washington, DC, US) **49**, 312 (2010).

[6] U. Ruschewitz, Coord. Chem. Rev. **244**, 115 (2003).

[7] M. Knapp and U. Ruschewitz, Chem. Eur. J. **7**, 874 (2001).

[8] V. Vohn, W. Kockelmann, and U. Ruschewitz, J. Alloys Compd. **284**, 132 (1999).

[9] X. Wang, I. Loa, K. Syassen, R. K. Kremer, A. Simon, M. Hanfland, and K. Ahn, Phys. Rev. B **72**, 064520 (2005).

[10] S. Karmakar, X. Wang, I. Efthimiopoulos, K. Syassen, V. Babizhetskyy, R. Kremer, and A. Simon (unpublished).

[11] J.-P. Dancausse, S. Heathman, U. Benedict, L. Gerward, J. S. Olsen, and F. Hulliger, J. Alloys Compd. **191**, 309 (1993).

[12]I. Efthimiopoulos, K. Kunc, S. Karmakar, K. Syassen, M. Hanfland, and G. Vajenine, Phys. Rev. B **82**, 134125 (2010).

[13]T. E. Weller, M. Ellerby, S. S. Saxena, R. P. Smith, and N. T. Skipper, Nat. Phys. **1**, 39 (2005).

[14]P. Fuentealba and A. Savin, J. Phys. Chem. A **104**, 10882 (2000).

[15]P. Zaleski-Ejgierd, M. Hakala, and P. Pyykkö, Phys. Rev. B **76**, 094104 (2007).

[16]J. Feng, B. Xiao, and J. Chen, Sci. China, Ser. B: Chem. **51**, 545 (2008).

[17]P. Srepusharawoot, A. Blomqvist, C. M. Araújo, R. H. Scheicher, and R. Ahuja, Phys. Rev. B **82**, 125439 (2010).

[18]H. K. Mao, J. Xu, and P. Bell, J. Geophys. Res. **91**, 4673 (1986).

[19]A. P. Hammersley, S. O. Svensson, M. Hanfland, A. N. Fitch, and D. Hausermann, High Pressure Res. **14**, 235 (1996).

[20]A. C. Larsen and R. B. Von Dreele, Los Alamos National Laboratory Report No. LAUR 86-748, 2004 (unpublished).

[21]M. Stackelberg, Z. Phys. Chem., Abt. B **9**, 437 (1930)

[22]G. E. Pringle and D. E. Noakes, Acta Crystallogr. Sect. B: Struct. Crystallogr. Cryst. Chem. **24**, 262 (1968).

[23]O. Reckeweg and F. J. DiSalvo, Z. Naturforsch., B: J. Chem. Sci. **63**, 530 (2008).

[24]A. Kulkarni, K. Doll, J. C. Schön, and M. Jansen, J. Phys. Chem. B **114**, 15573 (2010).

[25]W. B. Holzapfel, Rep. Prog. Phys. **59**, 29 (1996).

[26]C. S. Yoo and M. Nicol, J. Phys. Chem. **90**, 6732 (1986).

[27]Takamura Kenichi, Phys. Rev. B **50**, 16238 (1994).

[28]K. Haller, J. H. Lunsford, and J. Laane, J. Phys. Chem. **100**, 551 (1996).

[29]D. de Waal, K.-J. Range, M. Königstein, and W. Kiefer, J. Raman Spectrosc. **29**, 109 (1998).

[30]J. P. Perdew, K. Burke, and M. Ernzerhof, Phys. Rev. Lett. **77**, 3865 (1996).

[31]P. E. Blöchl, Phys. Rev. B **50**, 17953 (1994).

[32]G. Kresse and D. Joubert, Phys. Rev. B **59**, 1758 (1999).

[33]G. Kresse and J. Hafner, Phys. Rev. B **47**, 558 (1993).

[34]G. Kresse and J. Furthmüller, Phys. Rev. B **54**, 11169 (1996).

[35]H. Monkhorst and J. Pack, Phys. Rev. B **13**, 5188 (1976).

[36]O. H. Nielsen and R. M. Martin, Phys. Rev. B **32**, 3780 (1985).

[37]S. Baroni, S. de Gironcoli, A. Dal Corso, and P. Giannozzi, Rev. Mod. Phys. **73**, 515 (2001).